Broad-spectrum inhibition of coronavirus main and papain-like proteases by HCV drugs

Brandon J. Anson
Department of Biological Sciences, Purdue University, West Lafayette, IN, USA.
Mackenzie E. Chapman
Department of Biological Sciences, Purdue University, West Lafayette, IN, USA.
Emma K. Lendy
Department of Biochemistry, Purdue University, West Lafayette, IN, USA.
Sergii Pshenychnyi
Recombinant Protein Production Core, Chemistry of Life Processes Institute, Northwestern 9 University, Evanston, IL, USA
Richard T. D'Aquila
Department of Medicine, Division of Infectious Diseases, Northwestern University, Feinberg School of Medicine, Chicago, IL, USA
Karla J. F. Satchell
Department of Microbiology-Immunology; Center for Structural Genomics of Infectious Diseases, Northwestern University, Feinberg School of Medicine, Chicago, IL, USA.
Andrew D. Mesecar (amesecar@purdue.edu)
Department of Biological Sciences; Department of Biochemistry, Purdue University, West Lafayette, IN, USA; Center for Structural Genomics of Infectious Diseases, Northwestern University, Feinberg School of Medicine, Chicago, IL, USA.

Research Article

Keywords: SARS-CoV-2, proteases, antiviral drugs screening, coronavirus 3CLpro enzymes inhibition

Posted Date: May 1st, 2020

DOI: https://doi.org/10.21203/rs.3.rs-26344/v1

Title: Broad-spectrum inhibition of coronavirus main and papain-like proteases by HCV drugs

Authors: Brandon J. Anson[1,†], Mackenzie E. Chapman[1,†], Emma K. Lendy[2,†], Sergii Pshenychnyi[3], Richard T. D'Aquila[4], Karla J. F. Satchell[5,6], Andrew D. Mesecar[1,2,6]*

Affiliations:

[1]Department of Biological Sciences, Purdue University, West Lafayette, IN, USA.

[2]Department of Biochemistry, Purdue University, West Lafayette, IN, USA.

[3]Recombinant Protein Production Core, Chemistry of Life Processes Institute, Northwestern University, Evanston, IL, USA.

[4]Department of Medicine, Division of Infectious Diseases, Northwestern University, Feinberg School of Medicine, Chicago, IL, USA.

[5]Department of Microbiology-Immunology, Northwestern University, Feinberg School of Medicine, Chicago, IL, USA.

[6]Center for Structural Genomics of Infectious Diseases, Northwestern University, Feinberg School of Medicine, Chicago, IL, USA.

*Correspondence to: Andrew D. Mesecar at amesecar@purdue.edu.

†These authors contributed equally to this work.

Abstract: Coronavirus disease 2019 (COVID-19) caused by SARS-CoV-2 has led to over 200,000 deaths thus far. We screened a library of approved antiviral drugs against the two SARS-CoV-2 proteases, 3C-like/main protease (3CLpro/Mpro) and papain-like protease (PLpro), which are essential for viral replication and attractive drug targets. Three HCV protease inhibitors were tested and found to inhibit 3CLpro and PLpro enzymes from *Alpha*-, *Beta*- and *Gamma-coronaviruses*. Anti-HIV drugs had no activity. Boceprevir and telaprevir inhibited 3CLpro, with boceprevir inhibiting eight of nine coronavirus 3CLpro enzymes tested including from SARS-CoV-2, MERS and SARS-CoV. Asunaprevir inhibited PLpro from SARS-CoV-2 and four other coronaviruses. The 1.4 Å X-ray structure of boceprevir bound to 3CLpro was determined to explain its broad-spectrum activity and guide structure-based design of inhibitors of multiple coronaviruses.

One Sentence Summary: A screen of approved antiviral drugs identified three HCV protease inhibitors, but no HIV protease inhibitors, as potential treatments for COVID-19, with the structure of boceprevir bound to 3CLpro revealing the molecular basis for its broad-spectrum efficacy across multiple coronaviruses.

A highly-infectious and lethal pandemic strain of a new coronavirus (SARS-CoV-2) emerged in December, 2019. SARS-CoV-2 is 82% identical to SARS-CoV based on their RNA genomes making them both members of the *Beta-coronavirus* genus. The exact clinical presentation of this new Coronavirus disease (COVID-19) is currently expanding, but so far it typically includes a lower respiratory tract infection, fever and fatigue (*1, 2*), along with less common symptoms including nausea, diarrhea (*3, 4*), anosmia (*5*), and aches. Serious cases present with pneumonia, acute respiratory distress syndrome (*6*), and sometimes acute kidney injury (*7*). Millions of people have been infected worldwide with a current case-fatality ratio between 3.5 to 15% depending on geographic location and factors not yet defined (*8*). To date, no antiviral drugs or vaccines have been approved to treat any human *Alpha-* or *Beta-coronavirus* infection. The urgency of a treatment for patients suffering from the COVID-19 pandemic is leading to a profusion of trials and even off-label use of regulatory agency approved drugs, often with minimal biological rationale. The immediate need for new interventions based on mechanistic understanding of pathogenesis has led to *in silico* and *in vitro* screening for drugs already approved for use, or already advanced in clinical trials, that can directly inhibit SARS-CoV-2.

A critical step in coronaviral replication is the processing of the orf1a and orf1ab polyproteins to the sixteen non-structural proteins required for the viral assembly vacuole, as well as for RNA transcription and genome replication. In SARS-CoV-2 and other coronaviruses this processing is achieved by the papain-like protease (PLpro) and 3C-like or main protease (3CLpro/Mpro). These two enzymes are each cysteine proteases essential for coronavirus replication and therefore are attractive drug targets; each has been successfully targeted previously by antiviral inhibitors (reviewed in (*9*)).

In this study, we targeted both proteases (PLpro and 3CLpro) from SARS-CoV-2 by first screening each enzyme against a library of FDA approved antiviral drugs or molecules in pharmaceutical development. We utilized well-established enzymatic assays for each protease (*9-11*) and first screened each enzyme for inhibition by drugs that are used to treat Hepatitis C virus (HCV) infections (Fig. 1). Among the 13 HCV drugs tested, only five were found to have significant inhibitory activity at a concentration of 100 μM and they were all HCV NS3/4A protease inhibitors. Two drugs, boceprevir and telaprevir, inhibited SARS-CoV-2 3CLpro activity at 98.7 ± 0.3% and 87.4 ± 2.6 %, respectively, but they did not inhibit PLpro. On the other hand, SARS-CoV-2 PLpro was inhibited by asunaprevir (78.0 ± 0.92 %), simeprivir (79.5 ± 1.3 %), and grazoprevir (78.0 ± 0.77 %), but these drugs did not inhibit 3CLpro. Boceprevir and telaprevir share a similar structural scaffold that is distinctively different than the scaffold shared by asunaprevir, simeprivir and grazoprevir (Fig. 2).

The FDA approved drugs boceprevir and telaprevir showed significant inhibition of 3CLpro from SARS-CoV-2 with IC_{50} values of 2.5 ± 0.05 μM and 10.7 ± 0.4 μM, respectively (Fig. 2a). The effectiveness of boceprevir as an inhibitor was unexpected as at least one computational study ranked boceprevir poorly on a molecule transformer-drug target interaction affinity score (*12*). We next tested the potency of boceprevir and telaprevir against a panel of eight other purified 3CLpro enzymes from the *Alpha-*, *Beta-*, and *Gamma*-coronaviral proteases, including the human coronaviruses SARS, MERS, NL63, HKU1; bat coronaviruses HKU4 and HKU5; and animal coronaviruses FIPV (cat) and IBV (bird). Remarkably, we found that

boceprevir inhibits eight out of the nine 3CLpro enzymes tested with IC_{50} values ranging from 420 nM to 9.2 μM, and that telaprevir inhibits six out of the nine 3CLpro enzymes with IC_{50} values ranging from 2.4 μM to 35 μM (Fig. 2a and Extended Data Fig. 1). Boceprevir exhibited equipotent inhibition of SARS-CoV-2 and SARS-CoV 3CLpro (IC_{50}s ~2.6 μM), which was expected given that their active sites are 100% identical (Extended Data Fig. 2).

The one exception to broad-spectrum inhibition of 3CLpro by boceprevir was the enzyme from seasonal NL63 coronavirus, which was weakly inhibited at concentrations up to 100 μM. In contrast, telaprevir inhibited 3CLpro from NL63 coronavirus with an IC_{50} of 19.1 ± 0.9 μM (Fig. 2a). Telaprevir also inhibited SARS-CoV-2 and SARS-CoV 3CLpro equipotently with IC_{50} values of 10.7 μM. It did not inhibit some of the 3CLpros that boceprevir did (3CLpro from MERS-CoV, HKU1 or FIPV). Although telaprevir did inhibit the enzymes from bat HKU4 and HKU5 coronaviruses, it exhibited little to no inhibition of the MERS-CoV 3CLpro. While the bat HKU4 and HKU5 3CLpros are 100% identical to MERS 3CLpro at their active sites, the enzyme from MERS-CoV is unique among them in exhibiting substrate-induced dimerization because it exists as a weakly associated dimer (*13*). HKU4 and HKU5 3CLpros on the other hand are tightly associated dimers (*14*). Boceprevir's interaction with MERS-CoV 3CLpro involves binding first to a monomer of MERS 3CLpro, thereby activating the enzyme via induced dimerization with an apparent K_a value of 230 ± 30 nM (Fig. 2a and Extended Data Fig. 1). Subsequently, boceprevir and free substrate compete for the second active site of the dimer with an IC_{50} value of 3.8 ± 0.4 μM, which is comparable to the IC_{50} values for the other 3CLpro enzymes (Fig.2a).

The three compounds that inhibit SARS-CoV-2 PLpro all have a similar peptidic backbone structures attached to a cyclopropyl sulfonamide group (Fig. 2b and Extended Data Fig. 3). Asunaprevir inhibited SARS-CoV-2 PLpro with an IC_{50} value of 53.9 ± 2.1 μM (Fig. 2b). Poor solubility of the less-active simeprivir and grazoprevir limited IC_{50} value determination. Danoprevir, which has a similar structure to asunaprevir and the other PLpro inhibitors, is inactive against SARS-CoV-2 PLpro with only 9% inhibition at a concentration of 100 μM. Next, we tested the ability of asunaprevir to inhibit PLpro and papain-like protease 2 (PLP2) from different *Alpha-* and *Beta-coronavirus*. The IC_{50} values for asunaprevir inhibition of five PLpros and PLP2s across the different genera of CoVs ranged from 31 to 59 μM suggesting it has broad-spectrum efficacy (Fig. 2b and Extended Data Fig. 1).

To unravel the structural basis for broad-spectrum inhibition of coronavirus 3CLpro, we determined the X-ray structure of boceprevir bound to the enzyme from SARS-CoV-2 to 1.45 Å with final R_{work} and R_{free} values of 19.1% and 20.3%, respectively (Extended Data Table 1). The electron density for boceprevir is clearly visible in the active site (Fig. 3a), and it forms a reversible, thiohemiketal adduct with the catalytic cysteine, Cys145, which is further stabilized by a hydrogen-bond with the sidechain of His41 (Fig. 3b) (*15*). Extensive hydrogen bonding occurs between boceprevir and SARS-CoV-2 3CLpro (Fig. 3b). Four out of five of these hydrogen bonds are with the peptide backbone. Most of these interactions are with residues that are 100% conserved among *Alpha-, Beta- and Gamma-coronaviruses* (Extended Data Fig. 2).

The terminal amide of boceprevir resides in a structurally confined S1' subsite which is part of the oxyanion hole, while the cyclobutyl group points into the S1 subsite (Fig. 3). The S1

subsite has fairly strict determinants in inhibitor specificity (*15*). Unlike most inhibitors and substrates that engage with His41 or Glu166 in the S1 subsite using hydrogen bonds (*9*), the cyclobutyl group of boceprevir is devoid of any hydrogen bonds thereby limiting the binding affinity of this drug. The S2 subsite is filled with the 6,6-dimethyl-3-azabicyclo[3.1.0]hexane group of boceprevir and is perhaps the greatest determinant of substrate and inhibitor specificity for coronavirus 3CLpro enzymes. This subsite is formed by the non-conserved S2 loop (*16*), which is a demonstrably important effector of specificity, both within this binding pocket and elsewhere in the enzyme (*17*). For coronavirus 3CLpros, there is no defined pocket or S3 subsite for a P3 group on a substrate or inhibitor. The backbone interactions between boceprevir and 3CLpro orient the P3 side chain of substrates and inhibitors into solvent making this a weak determinant of specificity (Fig. 3). The *t*-butyl moiety of boceprevir lies in the substrate P3 position and extends into solvent or S3 "subsite". The structure of the terminal *t*-butyl urea group on boceprevir is highly complementary with the S4 subsite pocket. The two NH groups on the urea linker form hydrogen bonds with the backbone carbonyl on Glu166 (Fig. 3b). This region has been only partially explored in the past for inhibitor development and those studies utilized covalent inhibitors (*18*).

Recently, Hilgenfeld and coworkers reported the 1.95Å crystal structure of SARS-CoV-2 bound to compound **13b** (*15*). Their work demonstrated the effectiveness of the α-ketoamide warhead for inhibiting 3CLpro and for blocking SARS-CoV-2 replication. When the crystal structures of SARS-CoV-2 bound to compound **13b** and boceprevir are superimposed, structural differences are observed (Fig. 4a). First, boceprevir has a cyclobutyl group in the P1 position instead of an (S)-γ-lactam glutamine residue that forms hydrogen bonds with side chain of Glu166 and backbone carbonyl of Phe140 (Fig. 3a). This difference alone could explain the 4-fold weaker affinity of boceprevir (IC_{50} =2.7 ± 0.05) compared to **13b** (0.67 ± 0.18 μM). However, the loss of two hydrogen bonds would be expected to cause a much larger reduction in affinity for boceprevir so there may be compensatory interactions between boceprevir and SARS-CoV-2 3CLpro that strengthen their interactions. For example, the two hydrogen bonds between the carbonyl oxygen of Glu166 and urea linker of boceprevir may help steer its *t*-butyl group into a better position in the S4 subsite strengthening the interaction with this site compared to **13b** (Fig. 4a). Another structural difference is the presence of the methylbenzyl group of **13b** that is attached to its α-ketoamide warhead. The presence of this group in **13b** fills the S1' pocket (Fig. 4a) and may contribute additional binding energy to this compound. It may also be that retaining such a large group in **13b** reduces its inhibitor potential compared to boceprevir (no additional group) or telaprevir which contains a smaller cyclopropyl group.

The difference in inhibitor potency between boceprevir and telaprevir and their binding to SARS-CoV-2 is only 4-fold (IC_{50} = 2.5 μM vs 10.7 μM). This enabled computational docking of telaprevir into the active site of SARS-CoV-2 and superimposing it with boceprevir (Fig. 4b). In addition, we included a superposition of the available 3CLpro structures from NL63, HKU1, HKU4, FIPV and IBV onto the structure of SARS-CoV-2 (Extended Data Fig. 5). The differences in the overall orientation of the boceprevir and telaprevir structures are small and the backbone of the inhibitors make the same contacts as shown in Fig. 3. The differences between these two compounds lie in their interactions with the subsites. The S1' subsite accommodates the cyclopropyl group of telaprevir well and its propyl group at the P1 position traces the cycylobutyl group of boceprevir into the S1 site. In the S2 subsite, the 1,2-

dimethyloctahydrocyclopenta[*c*]pyrrole fills the site in a similar manner as the 6,6-dimethyl-3-azabicyclo[3.1.0]hexane group of boceprevir does. The cyclohexyl group of telaprevir fits into the S4 site and overlays onto the *t*-butyl group of boceprevir. Finally, the pyrazine-2-carboxamido group at the terminus of telaprevir extends into solvent along with the t-butyl group in the P3 position (Fig. 4b).

The observation that boceprevir inhibits eight out of the nine coronavirus 3CLpros is significant because it suggests that it has potential as a broad-spectrum therapeutic. The recent work by Hilgenfeld and colleagues may help explain why the exception is the lack of inhibition of NL63 3CLpro by boceprevir (*19*). In that study, they substituted a series of alkyl groups at the P2 position to make **13b**-like analogs and they then compared the inhibitory potencies of these compounds against SARS and NL63 3CLpro. They found that larger groups, e.g. methylcyclopentane or methylcyclohexane, in that position produced a larger separation in the IC_{50} values compared to smaller groups. Through X-ray structural analysis, it was shown that the S2 subsite of SARS-CoV 3CLpro is much larger than the S2 subsite of NL63 (Extended Data Fig. 5a). This is the most plausible explanation for the difference in boceprevir binding to SARS-CoV-2 and NL63 enzymes. The amino acids in the S2 subsites of *Alpha-coronaviruses* differ vary in type and number from the *Beta-* and *Gamma-coronaviruses* (Fig. 4c).

The aforementioned explanation however fails to explain the fact that telaprevir, which has a large P2 group that is almost identical in molecular molar volume to the P2 group in boceprevir, is able to inhibit both SARS-CoV-2 and NL63 3CLpro. It is quite possible that the molecular shape difference is the explanation. It was shown by Zhang et al. that a **13b**-like analog containing a linear butane group was unable to inhibit NL63 3CLpro, but inhibitors with isobutane, methylcyclopropane or methylcyclobutane groups did inhibit NL63 (*19*). The inability of telaprevir to inhibit 3CLpro from FIPV or weakly inhibit IBV may stem from the structural differences in their S2 subsites combined with variations in their S1' subsites (Fig. 4b, 4c, and Extended Data Fig. 5b).

We also screened SARS-CoV-2 3CLpro and PLpro, which are cysteine proteases, against a small library of 20 drugs that are used or were developed to treat human immunodeficiency virus (HIV) infections. Earlier computational studies suggested that HIV protease inhibitors, although designed to specifically inhibit HIV's aspartyl protease, docked into the 3CLpro active site (*20-24*). Neither 3CLpro nor PLpro were inhibited significantly (<20%) by any of the HIV drugs tested, including any HIV protease inhibitor (Extended Data Fig. 6). We also tested famotidine (Pepcid®), a non-HIV drug that recently went into clinical trials for treatment of COVID-19, for inhibition of SARS-CoV-2 3CLpro and PLpro and it did not inhibit (<15% inhibition) either enzyme at a concentration of 200 μM.

The discovery that FDA approved drugs boceprevir and telaprevir have broad-spectrum activity against 3CLpros from multiple coronaviruses provides a potential foundation on which structure-based drug design can lead to more potent antiviral drugs for treatment of SARS-CoV-2, MERS, and other emerging or re-emerging coronavirus infections. Knowledge of the structural determinants for inhibitor potency from this work, and the recent work of others, provide critical information for such structure-based optimization of candidate therapeutics (*15, 25, 26*). In addition to the moderate enzyme inhibition shown here, neither boceprevir nor

telaprevir have been tested for impact on SARS-CoV-2 virus replication *in vitro*. Both drugs were withdrawn from the market as they were supplanted as HCV therapeutics by more potent and safer alternatives. Given these facts, we emphasize that boceprevir and telaprevir are not themselves good candidates for clinical development. Rather, their structural scaffolds have the potential to be rapidly optimized into potential clinical candidates. In addition, the results presented here showing no inhibition of either SARS-CoV-2 protease by lopinavir or any other HIV protease inhibitor are consistent with the lack of difference from standard of care in mortality, clinical improvement or detectable SARS-CoV-2 nasopharyngeal swab RNA in a randomized clinical trial of lopinavir-ritonavir in hospitalized patients (*27*). There are currently no laboratory or clinical data to support clinical trials or off-label use of HIV or HCV protease inhibitors for treatment of COVID-19.

References

1. C. Huang *et al.*, Clinical features of patients infected with 2019 novel coronavirus in Wuhan, China. *Lancet* **395**, 497-506 (2020).
2. L. L. Ren *et al.*, Identification of a novel coronavirus causing severe pneumonia in human: a descriptive study. *Chin Med J (Engl)*, (2020).
3. X. Jin *et al.*, Epidemiological, clinical and virological characteristics of 74 cases of coronavirus-infected disease 2019 (COVID-19) with gastrointestinal symptoms. *Gut*, (2020).
4. E. Poggiali, P. M. Ramos, D. Bastoni, A. Vercelli, A. Magnacavallo, Abdominal Pain: A Real Challenge in Novel COVID-19 Infection. *Eur J Case Rep Intern Med* **7**, 001632 (2020).
5. S. B. Gane, C. Kelly, C. Hopkins, Isolated sudden onset anosmia in COVID-19 infection. A novel syndrome? *Rhinology*, (2020).
6. L. Gattinoni, D. Chiumello, S. Rossi, COVID-19 pneumonia: ARDS or not? *Crit Care* **24**, 154 (2020).
7. V. Fanelli *et al.*, Acute kidney injury in SARS-CoV-2 infected patients. *Crit Care* **24**, 155 (2020).
8. C. R. Center. (Johns Hopkins School of Medicine, 2020), vol. 2020.
9. A. K. Ghosh, M. Brindisi, D. Shahabi, M. E. Chapman, A. D. Mesecar, Drug Development and Medicinal Chemistry Efforts Toward SARS□Coronavirus and Covid□19 Therapeutics. *ChemMedChem* **in press**, (2020).
10. Y. M. Báez-Santos, S. E. St John, A. D. Mesecar, The SARS-coronavirus papain-like protease: structure, function and inhibition by designed antiviral compounds. *Antiviral Res* **115**, 21-38 (2015).
11. V. Grum-Tokars, K. Ratia, A. Begaye, S. C. Baker, A. D. Mesecar, Evaluating the 3C-like protease activity of SARS-Coronavirus: recommendations for standardized assays for drug discovery. *Virus Res* **133**, 63-73 (2008).
12. B. R. Beck, B. Shin, Y. Choi, S. Park, K. Kang, Predicting commercially available antiviral drugs that may act on the novel coronavirus (SARS-CoV-2) through a drug-target interaction deep learning model. *Comput Struct Biotechnol J* **18**, 784-790 (2020).
13. S. Tomar *et al.*, Ligand-induced Dimerization of Middle East Respiratory Syndrome (MERS) Coronavirus nsp5 Protease (3CLpro): IMPLICATIONS FOR nsp5 REGULATION AND THE DEVELOPMENT OF ANTIVIRALS. *J Biol Chem* **290**, 19403-19422 (2015).
14. S. E. St John, S. Tomar, S. R. Stauffer, A. D. Mesecar, Targeting zoonotic viruses: Structure-based inhibition of the 3C-like protease from bat coronavirus HKU4--The likely reservoir host to

the human coronavirus that causes Middle East Respiratory Syndrome (MERS). *Bioorg Med Chem* **23**, 6036-6048 (2015).
15. L. Zhang *et al.*, Crystal structure of SARS-CoV-2 main protease provides a basis for design of improved α-ketoamide inhibitors. *Science*, (2020).
16. S. E. St John, B. J. Anson, A. D. Mesecar, X-Ray Structure and Inhibition of 3C-like Protease from Porcine Epidemic Diarrhea Virus. *Sci Rep* **6**, 25961 (2016).
17. T. Muramatsu *et al.*, SARS-CoV 3CL protease cleaves its C-terminal autoprocessing site by novel subsite cooperativity. *Proc Natl Acad Sci U S A* **113**, 12997-13002 (2016).
18. S. E. St John *et al.*, X-ray structure and inhibition of the feline infectious peritonitis virus 3C-like protease: Structural implications for drug design. *Bioorg Med Chem Lett* **25**, 5072-5077 (2015).
19. L. Zhang *et al.*, alpha-Ketoamides as Broad-Spectrum Inhibitors of Coronavirus and Enterovirus Replication: Structure-Based Design, Synthesis, and Activity Assessment. *J Med Chem*, (2020).
20. Y. W. Chen, C. B. Yiu, K. Y. Wong, Prediction of the SARS-CoV-2 (2019-nCoV) 3C-like protease (3CL (pro)) structure: virtual screening reveals velpatasvir, ledipasvir, and other drug repurposing candidates. *F1000Res* **9**, 129 (2020).
21. S. A. Khan, K. Zia, S. Ashraf, R. Uddin, Z. Ul-Haq, Identification of chymotrypsin-like protease inhibitors of SARS-CoV-2 via integrated computational approach. *J Biomol Struct Dyn*, 1-10 (2020).
22. V. Nukoolkarn, V. S. Lee, M. Malaisree, O. Aruksakulwong, S. Hannongbua, Molecular dynamic simulations analysis of ritonavir and lopinavir as SARS-CoV 3CL(pro) inhibitors. *J Theor Biol* **254**, 861-867 (2008).
23. J. T. Ortega, M. L. Serrano, F. H. Pujol, H. R. Rangel, Unrevealing sequence and structural features of novel coronavirus using in silico approaches: The main protease as molecular target. *EXCLI J* **19**, 400-409 (2020).
24. X. W. Zhang, Y. L. Yap, Old drugs as lead compounds for a new disease? Binding analysis of SARS coronavirus main proteinase with HIV, psychotic and parasite drugs. *Bioorg Med Chem* **12**, 2517-2521 (2004).
25. W. Dai *et al.*, Structure-based design of antiviral drug candidates targeting the SARS-CoV-2 main protease. *Science*, (2020).
26. Z. Jin *et al.*, Structure of M(pro) from COVID-19 virus and discovery of its inhibitors. *Nature*, (2020).
27. B. Cao *et al.*, A Trial of Lopinavir-Ritonavir in Adults Hospitalized with Severe Covid-19. *N Engl J Med*, (2020).

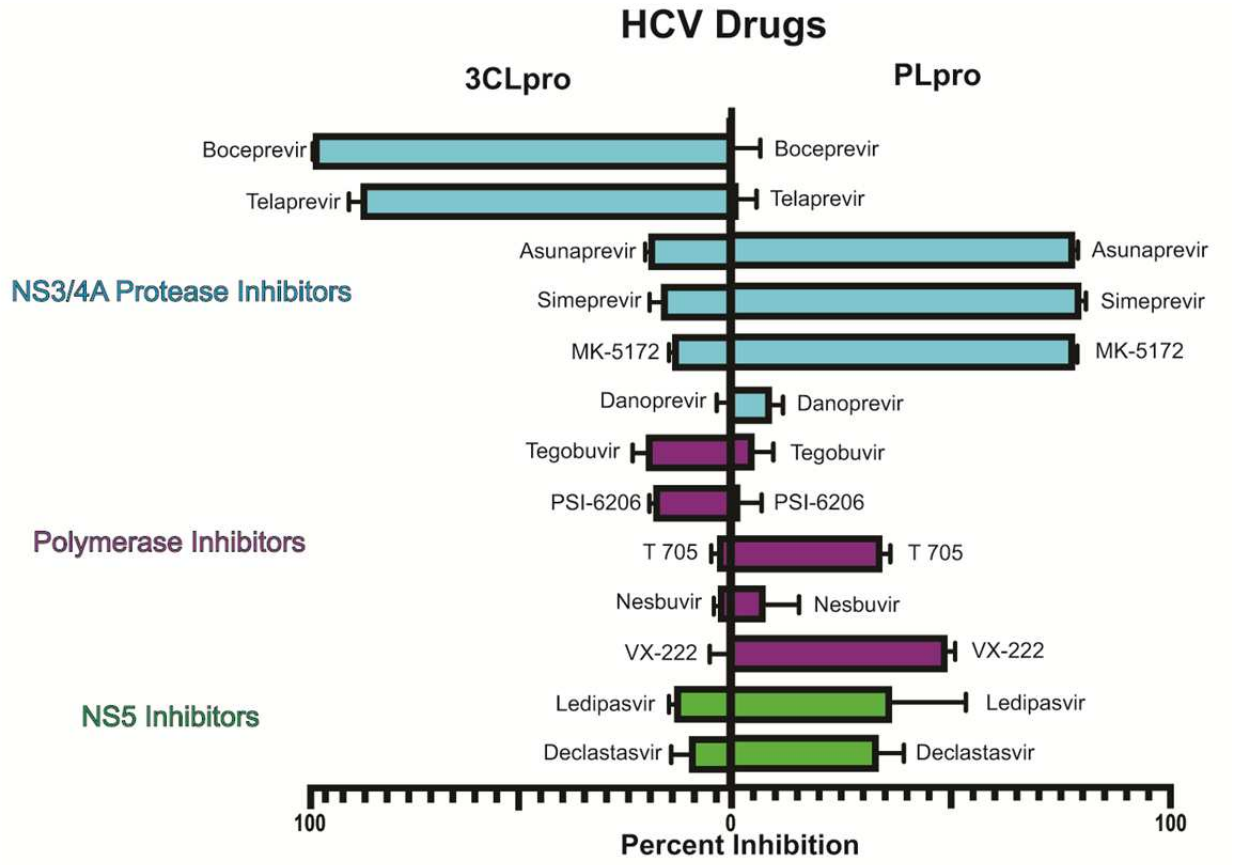

Fig. 1. Screening of SARS-CoV-2 proteases for inhibition by HCV drugs. Percent inhibition of each protease (3CLpro and PLpro) at a concentration of 100 μM for each HCV drug was determined by an enzymatic activity assay optimized for each enzyme. HCV drug classes are indicated and are distinguished by individual colors that correspond to the bar graph.

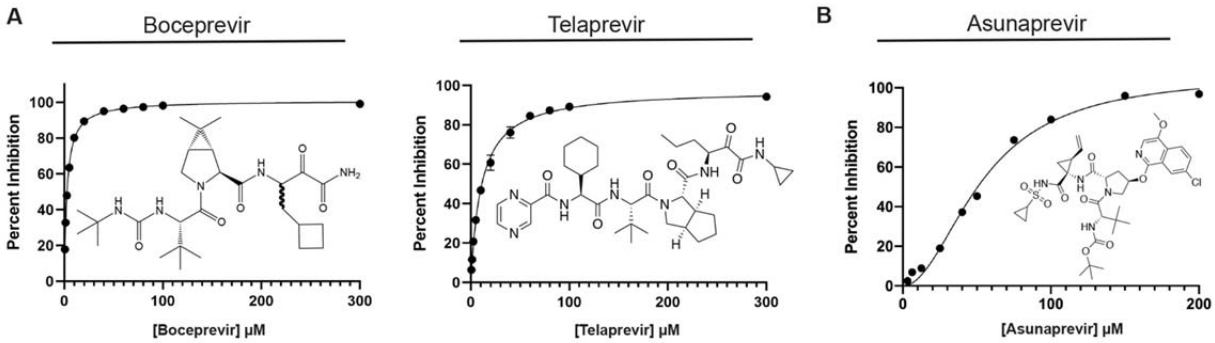

3CLpro	Boceprevir IC_{50}(μM)	Telaprevir IC_{50}(μM)
Beta-CoV		
SARS-CoV-2	2.7 ± 0.05	10.7 ± 0.4
SARS	2.5 ± 0.08	10.7 ± 0.5
MERS	3.8 ± 0.40	>100
HKU1	9.2 ± 2.1	>100
HKU4	0.42 ± 0.01	2.4 ± 0.2
HKU5	1.2 ± 0.03	8.7 ± 0.7
Alpha-CoV		
NL63	~100	19.1 ± 0.9
FIPV	3.9 ± 0.4	>100
Gamma-CoV		
IBV	2.4 ± 0.05	34.8 ± 2.6

PLpro/PLP2	Asunaprevir IC_{50}(μM)
Beta-CoV	
SARS-CoV-2	53.9 ± 2.1
SARS	47.8 ± 2.3
MERS	41.8 ± 7.4
MHV	29.6 ± 1.4
Alpha-CoV	
NL63	58.8 ± 2.0
FIPV	31.1 ± 9.4
PEDV	49.0 ± 1.3

Fig. 2. Inhibition of *Alpha-*, *Beta-* and *Gamma-coronavirus* 3CLpro and PLpro proteases by top HCV drugs. **A)** Dose-response of SARS-CoV-2 3CLpro to inhibition by Boceprevir and Telaprevir. Structures of each compound are shown with the dose-response curves. The IC_{50} values for each compound are listed. The response of each enzyme to the binding of the drugs follows a simple dose-response curves described by the Michaelis-Menten equation. **B)** The IC_{50} values for inhibition of SARS-CoV-2 PLpro and other PLpros or PLP2s by asunaprevir are listed and were derived from fits of the data to the Michaelis-Menten and Hill equations. The dose-response curves for each 3CLpro and PLpro are given in the supplementary material.

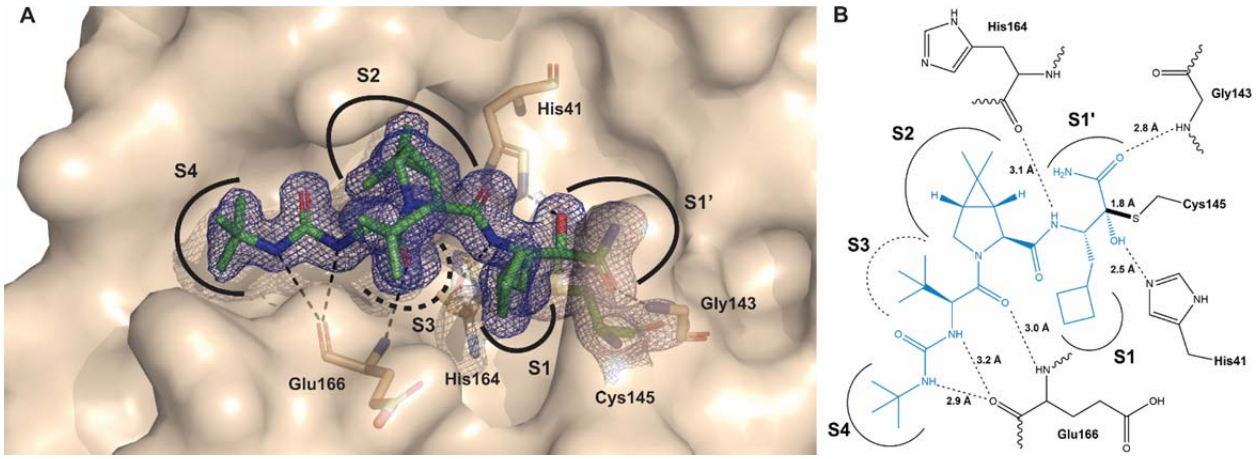

Fig. 3. Reversible covalent adduct of boceprevir bound to SARS-CoV-2 3CLpro. **A)** Final 1.45 Å structure of boceprevir bound to SARS-CoV-2 3CLpro. $2(F_o-F_c)$ electron density map is contoured at 1.0σ (blue mesh). Residues that form hydrogen bonds with the Boceprevir-modified cysteine (green) are rendered in brown with hydrogen bonds depicted by black dashed lines. The locations of subsites S1', S1, S2 and S4 are illustrated by black curves. The S3 "subsite" is solvent exposed. **B)** Schematic of hydrogen-bonding interactions between boceprevir and SARS-CoV-2 3CLpro. Boceprevir (blue) forms a reversible covalent bond (black, bold line) with the catalytic Cys145. SARS-CoV-2 3CLpro residues that hydrogen bond to boceprevir are depicted in black.

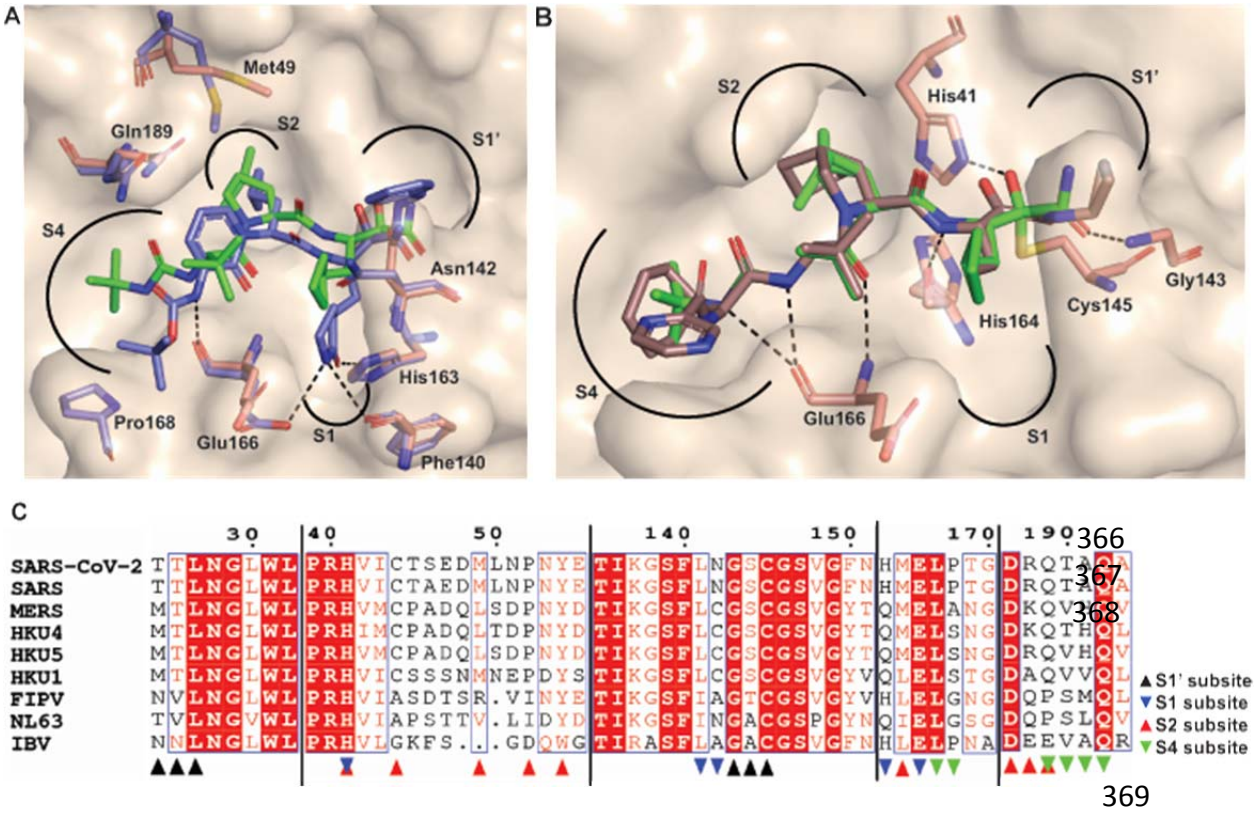

Fig. 4. Subsite binding interactions of Boceprevir, Telaprevir, and Compound **13b** with SARS-CoV-2 3CLpro. **A)** Structural alignment of SARS-CoV-2 3CLpro bound to boceprevir (PDB: 6WNP) and compound **13b** (PDB: 6Y2F). A surface representation of SARS-CoV-2 3CLpro bound to boceprevir is shown with selected amino acid side chains shown in pink and boceprevir in green. Compound **13b** and amino acid side chains are represented in purple. Subsites S1', S1, S2, and S4 are identified. Rendered amino acids illustrate the differences in conformation between boceprevir-bound and **13b**-bound SARS-CoV-2 3CLpro. Hydrogen bonds in the S1 and S4 subsites are shown as black, dashed lines. **B)** Surface representation of SARS-CoV-2 3CLpro is shown with boceprevir (green) bound. Telaprevir (brown) is modeled into the active site and superimposed on the boceprevir-bound structure. Subsites are identified and amino acids shown in pink are residues that participate in hydrogen bonding with both Boceprevir and Telaprevir. **C)** Sequence alignment and subsite identification of *Alpha*-, *Beta*-, and *Gamma-coronavirus* 3CLpro enzymes included in this study. Residues in the S1' site are shown in black (▲), S1 in blue (▼), S2 in red (▲), and S4 in green (▼). Sequences numbered according to SARS-CoV-2 3CLpro.

Methods

Expression and purification of *Alpha*-, *Beta*-, and *Gamma-coronavirus* 3CLpro enzymes

The gene encoding the 3CLpro of SARS-CoV-2 was obtained from the polyprotein sequence (Accession #: MN908947) and was verified against additional sequences obtained from the Global Initiative on Sharing All Influenza Data (GISAID) (Accession #'s: 402119-402125). The plasmid gene insert was designed to include codons for an N-terminal hexahistidine tag following the initiator methionine. This was followed by polyprotein residues 3259-3569 to reflect the sequence of the 3CLpro enzyme in addition to the nsp4/5 autocleavage site. This gene sequence was codon-optimized for expression in *E. coli* and subcloned into a pET11a vector using the synthetic DNA services of Bio Basic, Inc. (Amherst, NY). These principles were applied to the expression construct design because it produces 3CLpro with native termini.

The plasmid containing the gene insert for overexpression of SARS-CoV-2 3CLpro was electroporated with *E. coli* BL21 (DE3) cells. A single colony of the transformed cells was used to inoculate 70 mL of 2xYT media (10 g yeast extract, 16 g tryptone, 5 g NaCl per 1 L of water, 100 μg/mL carbenicillin, pH adjusted to 7.20 using 10 M NaOH). This preculture was incubated overnight at 37 °C for 10.5 hours. The expression culture consists of 1L 2xYT media supplemented with 10 mL of preculture and incubated at 37 °C for 3.25 hours. When the cells reached an OD_{600} of 0.72, the cultures were incubated on ice for 15 minutes before supplementation with isopropyl β-D-1-thiogalactopyranoside (IPTG) to a final concentration of 0.1 mM. These cultures were incubated for 16 h at 25 °C. The cells were harvested via centrifugation at 16,800 x g for 40 minutes to yield 5.09 g L^{-1} of cells. The cell pellet was resuspended in 5 mL Lysis Buffer (25 mM HEPES, 0.05 mM EDTA, 5 mM β-mercaptoethanol (β-ME), 1 mg/mL lysozyme) per 1 g of pelleted cells using a manual homogenizer. The

417 homogenized cell suspension was sonicated for a total of 12 minutes at an amplitude of 60% for
418 periods of 10 s punctuated by 20 s delays using a Branson digital sonifier. The lysate produced
419 was clarified by centrifugation for 16,080 x g for 45 minutes at 4 °C.
420 Clarified lysate was injected onto a 60 mL Q-Sepharose Fast Flow (GE Healthcare)
421 strong anion-exchange column equilibrated in Buffer A (25 mM HEPES pH 7.50, 0.05 mM
422 EDTA, 5 mM β-ME). Protein was recovered from the flow-through. Solid ammonium sulfate
423 was gradually added to the protein pool to a concentration of 1 M while stirring on ice. The
424 precipitate was removed via centrifugation at 16,080 x g for 45 minutes at 4 °C. Supernatant was
425 checked for activity prior to injection onto a 60 mL Phenyl Sepharose 6 Fast Flow Hi Sub (GE
426 Healthcare) hydrophobic interaction column that had been equilibrated in Buffer B (50 mM
427 HEPES pH 7.50, 1 M ammonium sulfate 0.05 mM EDTA, 5 mM β-ME). The protein was eluted
428 using a linear gradient to 100% Buffer A over 14 column volumes. Fractions containing SARS-
429 CoV-2 3CLpro were assessed for purity and pooled based on specific activity and analysis via
430 SDS-PAGE. This protein was syringe-filtered with a 0.45 μm surfactant free cellulose acetate
431 membrane prior to injection onto an 8 mL Mono Q column (GE Healthcare) equilibrated in
432 Buffer A for anion-exchange chromatography. The protein was eluted using a gradient to 100%
433 Buffer C (50 mM HEPES pH 7.50, 1 M NaCl, 0.05 mM EDTA, 5 mM β-ME) over 20 column
434 volumes. Fractions were pooled using the same criteria. This pool was concentrated using a
435 10,000 molecular weight cutoff (MWCO) spin concentrator (MilliporeSigma) before being
436 injected onto a 300 mL HiLoad 26/60 Superdex 200 prep grade column (GE Healthcare) for
437 size-exclusion and desalting into Buffer E (25 mM HEPES pH 7.50, 10% Glycerol, 2.5 mM
438 dithiothreitol (DTT)). The protein was pooled based on the above criteria, aliquoted, flash-frozen
439 in liquid nitrogen, and stored at -80 °C.

SARS, HKU1, HKU5 and MERS 3CLpro were expressed and purified utilizing the protocols developed by Dr. Sakshi Tomar (*28*). NL63 3CLpro was expressed and purified using a modified protocol based on the purification of murine hepatitis virus (MHV) 3CLpro using DEAE-Cellulose columns (*28*). Avian coronavirus (IBV) 3CLpro was expressed and purified using a modified protocol based on MERS 3CLpro (28). HKU4 3CLpro was expressed and purified using a modified protocol developed by Agnihothram et al (*29*). Feline infectious peritonitis virus (FIPV) 3CLpro was expressed and purified using the protocol developed by St. John et al (*18*). Molar concentration and experimental ε_{280} of 3CLpro was determined spectroscopically using a Synergy H1 hybrid multi-mode plate reader (Biotek) utilizing the method described by Gill & von Hippel (*30*).

Crystallization of SARS-CoV-2 3CLpro

Protein was thawed and injected onto a 24 mL Superdex 200 10/300 GL (GE Healthcare) equilibrated in Buffer F (25 mM HEPES pH 7.50, 2.5 mM DTT) for polishing and desalting. SARS-CoV-2 3CLpro was pooled based upon specific activity and SDS-PAGE and concentrated using a 10,000 MWCO spin concentrator (MilliporeSigma) to 4.7 mg/mL for crystallization optimization in 24-well hanging drop VDX trays (Hampton Research). Concentrations of KCl and PEG-10,000 were varied along with drop ratios of protein and reservoir solution 1:2, 1:1, 2:1. Crystals grew at 4 °C in a droplet containing 2.67 mM DTT, 0.33% hexylene glycol (MPD), 16.67 mM MES pH 6.0, 26.67 mM KCl, 5.33% PEG-10,000, 16.67 mM HEPES pH 7.50, 0.67% dimethyl sulfoxide (DMSO) and 200 μM Boceprevir. These were transferred to a cryo-solution containing 1.33 mM DTT, 15.17 % MPD, 8.33 mM MES pH 6.0, 13.33 mM KCl, 2.67 % PEG-10,000, 20.84 mM HEPES pH 7.50, 0.84% DMSO and 250 μM Boceprevir, then allowed to soak for 90 minutes prior to flash-freezing in liquid nitrogen in 0.05-0.1 μm nylon loops.

Data collection and structure refinement of SARS-CoV-2 3CLpro

X-ray diffraction data were collected at Life Sciences Collaborative Access Team (LS-CAT) beamline 21-ID-F at the Advanced Photon Source (APS) at Argonne National Laboratory, Argonne, Illinois, USA. These data were indexed and integrated using Denzo and scaled using Scalepack as part of the HKL-2000 package(*31*). The structure factor amplitudes were used for molecular replacement in the Phaser-MR (full-interface) module of PHENIX(*32*). The search model used was an X-ray structure of SARS-CoV-2 3CLpro (RCSB: 6LU7)(*3*) with ligands and models removed. Several iterations of automated structural refinement were completed using the PHENIX refinement module and REFMAC while manual adjustments were made using Coot(*33*). Table S1 summarizes the final diffraction and refinement statistics.

Inhibitor characterization of SARS-CoV 3CLpro

All compounds, unless otherwise noted, were obtained from the APExBIO (Boston, MA) as part of their DiscoveryProbe™ Anti-virus Compound library. Lopinavir, Darunavir and Maraviroc were also obtained from Prof. Arun Ghosh, Purdue University. Inhibition of SARS-CoV-2 (200 nM), SARS (250 nM), MERS (1 μM), HKU4 (100 nM), HKU5 (125 nM), HKU1 (125 nM), FIPV (50 nM), NL63 (250 nM) and IBV 3CLpro (50 nM) by these compounds was assessed using a continuous kinetic assay measuring cleavage at 2 μM of the custom-synthesized FRET-based substrate: UIVT3 (HiLyte $Fluor_{488}$™–ESATLQSGLRKAK-QXL_{520}™-NH_2) (Anaspec) in Assay Buffer (50 mM HEPES pH 7.50, 0.1 mg/mL bovine serum albumin (BSA), 0.01% Triton X-100, 2 mM DTT, 1% DMSO). Inhibitor concentrations for Lopinavir, Darunavir and Maraviroc were assayed at concentrations of 0, 2.5, 5, 10, 15, 20, 40, 60, 80, 100, 150 and 200 μM and substrate concentration was 2 μM. IC_{50} assays were performed using Costar 3694 EIA/RIA 96-well half-area, flat bottom, black polystyrene plates (Corning). 1 μL of 100x

inhibitor stocks were prepared in DMSO and added to 79 µL of enzyme prepared in Assay Buffer prior to incubation at 25 °C and 37 °C for 10 minutes on an orbital shaker (Thermo Fisher Scientific) on low speed. The reaction was initiated by adding 20 µL of the UIVT3 substrate. Increase in fluorescence intensity of the reaction was measured with an λ_{ex} of 485/20 nm and an λ_{em} of 528/20 nm for a period of 10 min. Relative Fluorescence Units (RFU) produced were plotted over time within the initial rate period of the reaction to yield RFU/s. Percent inhibition of SARS-CoV-2 3CLpro by each inhibitor was calculated using equation (1).

Equation (1) $$\%\ Inhibition = 100 * [1 - \frac{Inhibited\ 3CL^{pro}\frac{RFU}{s} - Background\frac{RFU}{s}}{Uninhibited\ 3CL^{pro}\frac{RFU}{s} - Background\frac{RFU}{s}}]$$

measured by plotting average percent inhibition values from assays performed in triplicate at varying inhibitor concentrations. Lopinavir, Darunavir and Maraviroc were assayed at concentrations of 0, 2.5, 5, 10, 15, 20, 40, 60, 80, 100, 150 and 200 µM. Boceprevir and Telaprevir were assayed at concentrations of 0, 0.625, 1.25, 2.5, 5, 10, 20, 40, 60, 80, 100 and 300 µM. These data were fit to equation (2) to determine the IC_{50} for each compound where $\%I_{max}$ is the maximum percent inhibition of 3CLpro. Errors in IC_{50} and $\%I_{max}$ values are those obtained from fitting of equation (2) to the data. Dose-response curves for MERS 3CLpro were evaluated by fitting to equation (3). Fitting was performed utilizing GraphPad Prism.

Equation (2) $$\%\ Inhibition = \frac{\%I_{max} * [Inhibitor]}{IC_{50} + [Inhibitor]}$$

Equation (3) $$\%\ Rate = \frac{\%V_{max} * [Inhibitor]}{K_{a,app} + [Inhibitor] * (1 + \frac{[Inhibitor]}{K_{i\ app}})}$$

SARS-CoV-2 PLpro Expression and Purification

HCoV SARS-CoV-2 pET15b-PLpro $Ubl2_{(1564-1874)}$ was transformed into *E. coli* BL21 (DE3) cells for protein expression using a Bio-Rad Gene Pulser electroporator. Transformants were plated out on a Luria-Bertani (LB) agar plate, supplemented with 100µg/mL carbenicillin at 37°C in an incubator and grown overnight. The transformed cells were inoculated into a 40mL LB starter culture (LB Broth (Lennox) EZMix^{TM}, Sigma) supplemented with 400µg/mL Ampicillin and 35µg/mL Kanamycin and grown overnight at 200rpm, 37°C. The main culture was inoculated from the whole starter culture. Four L of cells containing HCoV SARS-CoV-2 pET15b-PLpro $Ubl2_{(1564-1874)}$ were grown at 37°C in Terrific Broth (TB) (Granulated, Fisher Scientific) supplemented with 400µg/mL ampicillin and 35 µg/mL kanamycin and incubated in BIOSTAT® Bplus Bioreactor (Sartorius Stedim). The initial fermentation conditions were set to a stirrer setpoint of 300rpm, temperature setpoint of 37°C, pH setpoint of 7.2 (± 0.2), gas flow setpoint of 3 L min^{-1}, and an O_2 setpoint of 20%. The cell culture was induced with 0.6 mM IPTG when OD_{600} reached 0.8 and incubated overnight at 25°C. After growth, the cells were pelleted by centrifugation (8000 x *g*, 15 min, 4 °C).

The cells were resuspended in lysis buffer (10mM Tris-HCl, 500mM NaCl, 5% glycerol, 5mM imidazole, 5mM β-ME, 0.08% *n*-Dodecyl β-D-maltoside (DDM), pH 7.4), homogenized in EmulsiFlex-C5 High Pressure Homogenizer (Avestin) two times and clarified by centrifugation (18000rpm, 40 min, 4°C). The purification was run using an AKTAxpress (GE Healthcare Life Science) pre equilibrated with Buffer A (10mM Tris-HCl, 500mM NaCl, 5mM β-ME, pH 7.4), washed with Buffer A with addition of 25 mM of Imidazole to remove unspecific binding and eluted with Buffer B (10mM Tris-HCl, 500mM NaCl, 500mM Imidazole, pH 7.4). Then, the sample was loaded onto a HiLoad 26/600 Superdex prep grade column (GE Healthcare Life Science) for size-exclusion and desalting into Buffer A). The selected fraction was incubated

with tobacco etch virus (TEV) protease in a 1:20 ratio for four hour a room temperature, and then 4°C overnight. The reaction was passed over a HiTrap FF column and the cleaved, untagged protein was collected from a 5 % imidazole step elution. The fractions were buffer exchanged by dialysis into a storage buffer (10 mM Tris-HCl, 500 mM NaCl, 5 mM β-ME, pH 7.4) and concentrated to ~5mg/mL in a Vivaspin Protein Concentrator Spin Column with MWCO 10,000 (GE Healthcare Life Science). During the purification, the protein concentration was evaluated on NanoDrop 2000 UV Spectrophotometer (ThermoScientific) and visualized on SDS-PAGE gels.

Other *Alpha-* and *Beta-Coronavirus* PLP2 and PLpro Expression and Purification

Methods for the expression and purification of MHV $PLpro_{1609-1911}$, SARS $PLpro_{1541-1855}$, and MERS $PLpro_{1484-1802}$ have been previously described (*34-36*). FIPV $PLP2_{1558-1794}$, Porcine epidemic diarrhea virus (PEDV) $PLP2_{1688-1933}$, and NL63 $PLP2_{1578-1897}$ were purified in similar ways using buffer conditions previously described.(*37*) All constructs were expressed in *E. coli* BL21 (DE3) by autoinduction using a medium containing LB (10 g NaCl, 5 g yeast extract, 10g tryptone, 3 g KH_2PO_4, 6 g Na_2HPO_4) and supplemented with 0.2 % lactose, 0.6 % glycerol, 0.05 % glucose, and 100 μg/mL carbenicillin. Cultures were grown at 37°C for 24 hours before being pelleted by centrifugation. The cells were resuspended in buffer A containing lysozyme by vortexing. The cells were then lysed for 8-10 minutes by sonication using a Branson Digital Sonifier and then clarified by centrifugation.

The clarified lysate was loaded onto a Ni^{2+} column equilibrated with buffer A. Unbound proteins were washed with buffer A and bound proteins were eluted with a 0-100 % gradient of buffer B. The His-tag was removed after incubation with TEV-protease and put over the Ni^{2+} column to separate out the untagged protein. The sample was then loaded onto a Superdex 75

HR 26/60 column equilibrated with buffer C. The protein eluted and was concentrated to 5-10 mg/mL. At every step of the purification, the protein concentration was calculated using a Bradford assay and the protein was analyzed on SDS-PAGE gels. Specific activity was determined throughout the entire purification.

Inhibition Assays of PLP2 and PLpro

Assays were performed in triplicate in a Costar 96-well black microplate, 100µL assay volume. The substrate used in this assay was the fluorogenic peptide Arg-Leu-Arg-Gly-Gly-AMC (RLRGG-AMC) (Bachem). The assay contained the following: 50 mM HEPES, pH 7.5, 0.1 mg/mL BSA, 5 mM DTT, 50 µM RLRGG-AMC, 1 % DMSO, and two concentrations of inhibitor (100 and 200 µM). The reaction was initiated with a final enzyme concentration of 0.14 µM for SARS- 2 PLpro $Ubl2_{(1564\text{-}1874)}$, SARS PLpro, NL63 PLP2, and PEDV PLP2 and a concentration of 1 µM for MERS PLpro, MHV PLpro, and FIPV PLP2. The enzyme activity was monitored using a CLARIOstar Plus Microplate Reader. Percent inhibition was calculated using previously derived equations, accounting for both a positive and negative control.(*38*) The data were then fit using Graph Pad Prism using both the Hill equation and Michaelis-Menten model to determine an IC_{50} value.

References

28. S. Tomar, Purdue University. Biological Sciences., *Understanding the determinants for substrate recognition, regulation of enzymatic activity and the development of broad-spectrum inhibitors of coronavirus 3-chymotrypsin-like proteases*. pp. 1 electronic resource (239 pages).
29. S. Agnihothram *et al.*, A mouse model for Betacoronavirus subgroup 2c using a bat coronavirus strain HKU5 variant. *mBio* **5**, e00047-00014 (2014).
30. S. C. Gill, P. H. von Hippel, Calculation of protein extinction coefficients from amino acid sequence data. *Anal Biochem* **182**, 319-326 (1989).
31. Z. Otwinowski, W. Minor, Processing of X-ray diffraction data collected in oscillation mode. *Methods Enzymol* **276**, 307-326 (1997).
32. P. D. Adams *et al.*, PHENIX: a comprehensive Python-based system for macromolecular structure solution. *Acta Crystallogr D Biol Crystallogr* **66**, 213-221 (2010).
33. P. Emsley, B. Lohkamp, W. G. Scott, K. Cowtan, Features and development of Coot. *Acta Crystallogr D Biol Crystallogr* **66**, 486-501 (2010).

34. Y. M. Báez-Santos, A. M. Mielech, X. Deng, S. Baker, A. D. Mesecar, Catalytic function and substrate specificity of the papain-like protease domain of nsp3 from the Middle East respiratory syndrome coronavirus. *J Virol* **88**, 12511-12527 (2014).
35. K. Ratia *et al.*, Severe acute respiratory syndrome coronavirus papain-like protease: structure of a viral deubiquitinating enzyme. *Proc Natl Acad Sci U S A* **103**, 5717-5722 (2006).
36. Y. Chen *et al.*, X-ray Structural and Functional Studies of the Three Tandemly Linked Domains of Non-structural Protein 3 (nsp3) from Murine Hepatitis Virus Reveal Conserved Functions. *J Biol Chem* **290**, 25293-25306 (2015).
37. J. R. Clasman *et al.*, X-ray Structure and Enzymatic Activity Profile of a Core Papain-like Protease of MERS Coronavirus with utility for structure-based drug design. *Sci Rep* **7**, 40292 (2017).
38. Y. C. Yen *et al.*, Development of an Efficient Enzyme Production and Structure-Based Discovery Platform for BACE1 Inhibitors. *Biochemistry* **58**, 4424-4435 (2019).

Acknowledgments: Members of the Center for Structural Genomics of Infectious Diseases and the NU Structural Biology Core are thanked for assistance. Thanks also to Dr. Joseph Brunzelle at LS-CAT for assistance with X-ray data collection.

Funding: This project has been funded in whole or in part with Federal funds from the National Institute of Allergy and Infectious Diseases, National Institutes of Health, Department of Health and Human Services, under Contract No. HHSN272201700060C and by award number R01AI085089 to ADM. MEC is supported by an NIH/NIGMS T32 Training Grant for Structural Biology and Biophysics (#GM132024). This research used resources of the Advanced Photon Source, a U.S. Department of Energy (DOE) Office of Science User Facility operated for the DOE Office of Science by Argonne National Laboratory under Contract No. DE-AC02-06CH11357. Use of the LS-CAT Sector 21 was supported by the Michigan Economic Development Corporation and the Michigan Technology Tri-Corridor (Grant 085P1000817). The contents of these studies are solely the responsibility of the authors and do not necessarily represent the official views of the NIAID, NIGMS or NIH.

Author contributions ADM, BA, MC, EL and KJFS contributed to conceptualization. BA, MC, EL, SP and ADM contributed to the investigations, formal analysis and methodology. MC, EL, BA and ADM contributed to visualization and/or data curation. ADM and KS contributed to funding acquisition, supervision, project administration and resources. All authors contributed to writing all drafts of the manuscript

Competing interests: K.S. has a significant financial interest in Situ Biosciences, LLC, a CRO that conducts testing of industrial products, including antiviral chemistries. R.T.D. has a contractual relationship with Abbvie on projects unrelated to drug development. A.D.M has a sponsored program contract with Pfizer to test compounds their compounds for inhibition of coronavirus proteases.

Data and materials availability: The X-ray structure reported here has been deposited to the RCSB Protein Data Bank under accession number 6W81. Plasmids used for protein expression are to be deposited and freely available from BEI Resources (beiresources.org).

Figures

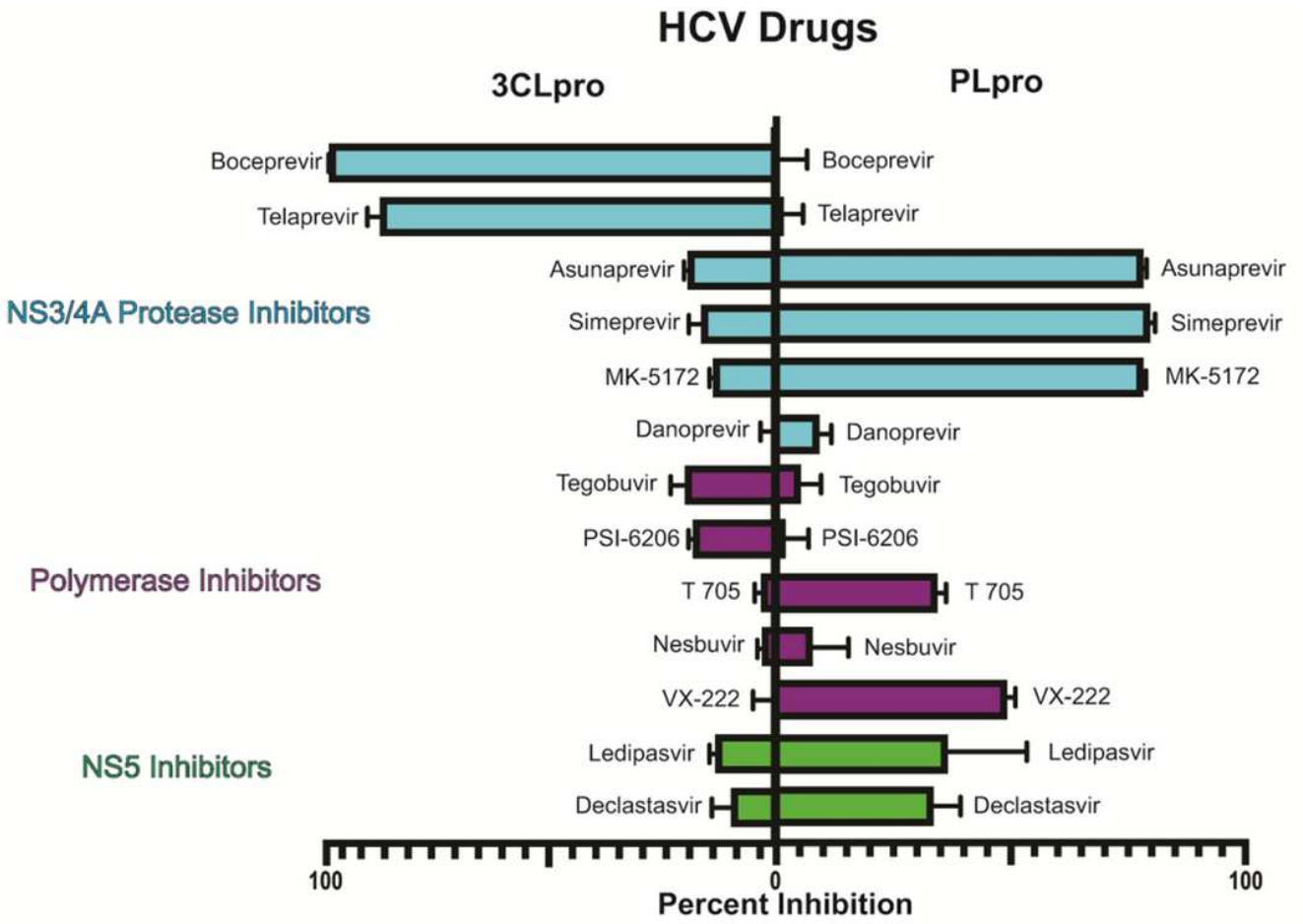

Figure 1

Screening of SARS-CoV-2 proteases for inhibition by HCV drugs. Percent inhibition of each protease (3CLpro and PLpro) at a concentration of 100 μM for each HCV drug was determined by an enzymatic activity assay optimized for each enzyme. HCV drug classes are indicated and are distinguished by individual colors that correspond to the bar graph.

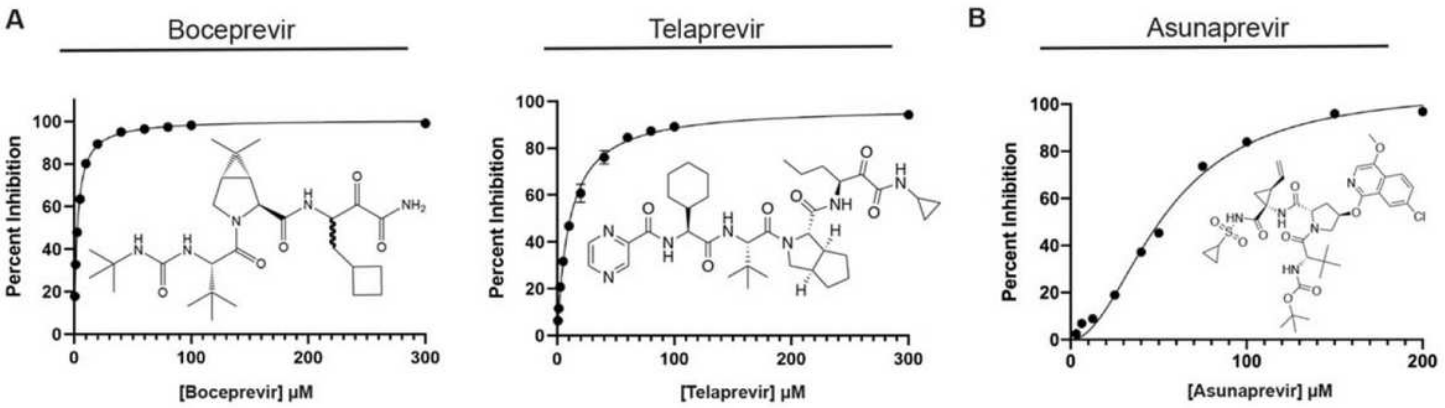

3CLpro	Boceprevir IC_{50}(μM)	Telaprevir IC_{50}(μM)
Beta-CoV		
SARS-CoV-2	2.7 ± 0.05	10.7 ± 0.4
SARS	2.5 ± 0.08	10.7 ± 0.5
MERS	3.8 ± 0.40	>100
HKU1	9.2 ± 2.1	>100
HKU4	0.42 ± 0.01	2.4 ± 0.2
HKU5	1.2 ± 0.03	8.7 ± 0.7
Alpha-CoV		
NL63	~100	19.1 ± 0.9
FIPV	3.9 ± 0.4	>100
Gamma-CoV		
IBV	2.4 ± 0.05	34.8 ± 2.6

PLpro/PLP2	Asunaprevir IC_{50}(μM)
Beta-CoV	
SARS-CoV-2	53.9 ± 2.1
SARS	47.8 ± 2.3
MERS	41.8 ± 7.4
MHV	29.6 ± 1.4
Alpha-CoV	
NL63	58.8 ± 2.0
FIPV	31.1 ± 9.4
PEDV	49.0 ± 1.3

Figure 2

Inhibition of Alpha-, Beta- and Gamma-coronavirus 3CLpro and PLpro proteases by top HCV drugs. A) Dose-response of SARS-CoV-2 3CLpro to inhibition by Boceprevir and Telaprevir. Structures of each compound are shown with the dose-response curves. The IC50 values for each compound are listed. The response of each enzyme to the binding of the drugs follows a simple dose-response curves described by the Michaelis-Menten equation. B) The IC50 values for inhibition of SARS-CoV-2 PLpro and other PLpros or PLP2s by asunaprevir are listed and were derived from fits of the data to the Michaelis-Menten and Hill equations. The dose-response curves for each 3CLpro and PLpro are given in the supplementary material.

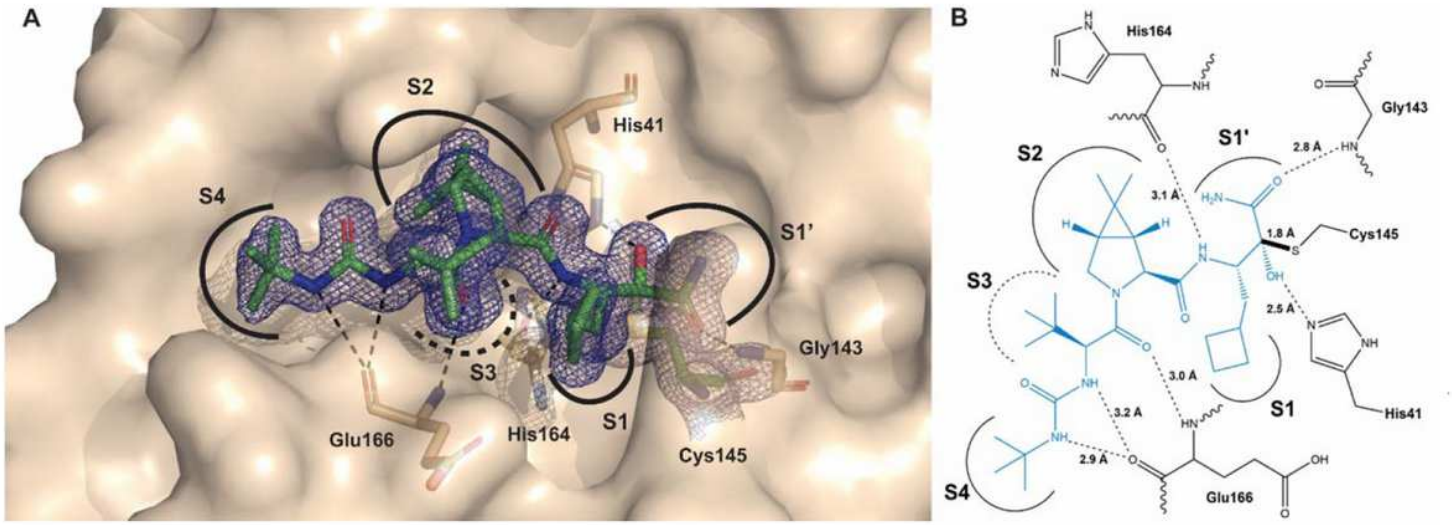

Figure 3

Reversible covalent adduct of boceprevir bound to SARS-CoV-2 3CLpro. A) Final 1.45 Å structure of boceprevir bound to SARS-CoV-2 3CLpro. 2(Fo-Fc) electron density map is contoured at 1.0σ (blue mesh). Residues that form hydrogen bonds with the Boceprevir-modified cysteine (green) are rendered in brown with hydrogen bonds depicted by black dashed lines. The locations of subsites S1', S1, S2 and S4 are illustrated by black curves. The S3 "subsite" is solvent exposed. B) Schematic of hydrogen-bonding interactions between boceprevir and SARS356 CoV-2 3CLpro. Boceprevir (blue) forms a reversible covalent bond (black, bold line) with the catalytic Cys145. SARS-CoV-2 3CLpro residues that hydrogen bond to boceprevir are depicted in black.

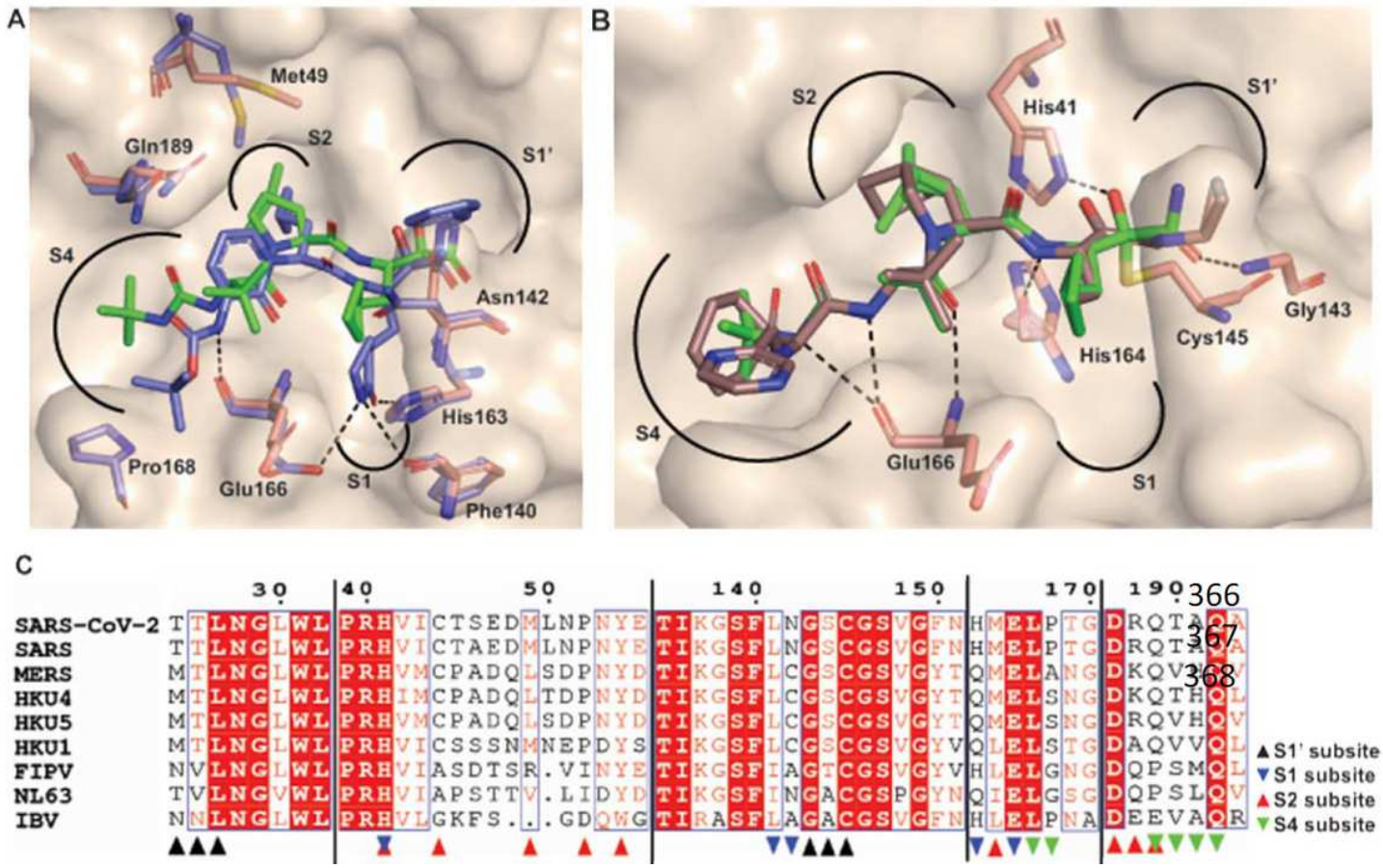

Figure 4

Subsite binding interactions of Boceprevir, Telaprevir, and Compound 13b with SARS371 CoV-2 3CLpro. A) Structural alignment of SARS-CoV-2 3CLpro bound to boceprevir (PDB: 6WNP) and compound 13b (PDB: 6Y2F). A surface representation of SARS-CoV-2 3CLpro bound to boceprevir is shown with selected amino acid side chains shown in pink and boceprevir in green. Compound 13b and amino acid side chains are represented in purple. Subsites S1', S1, S2, and S4 are identified. Rendered amino acids illustrate the differences in conformation between boceprevir-bound and 13b-bound SARS-CoV-2 3CLpro. Hydrogen bonds in the S1 and S4 subsites are shown as black, dashed lines. B) Surface representation of SARS-CoV-2 3CLpro is shown with boceprevir (green) bound. Telaprevir (brown) is modeled into the active site and superimposed on the boceprevir-bound structure. Subsites are identified and amino acids shown in pink are residues that participate in hydrogen bonding with both Boceprevir and Telaprevir. C) Sequence alignment and subsite identification of Alpha-, Beta-, and Gamma-coronavirus 3CLpro enzymes included in this study. Residues in the S1' site are shown in black (▲), S1 in blue (▼), S2 in red (▲), and S4 in green (▼). Sequences numbered according to SARS-CoV-2 3CLpro.

Supplementary Files

This is a list of supplementary files associated with this preprint. Click to download.

- 20200407332AED.pdf